Proceedings of the
Annual Stability Conference
Structural Stability Research Council
Louisville, Kentucky, April 1-4, 2025

The modal finite strip method (mFSM) for buckling mode decomposition in built-up members: applications and examples

Mani Khezri[1], Kim J.R. Rasmussen[2]

Abstract
This paper investigates the practical applications of the Modal Finite Strip Method (mFSM) to the buckling mode decomposition of built-up thin-walled members. Building upon the Authors' previous work, which introduced the underpinning decomposition technique, this study presents a comprehensive investigation into several of the diverse range of applications enabled by the proposed method. The effectiveness and versatility of the decomposition method are demonstrated through numerical studies of a built-up column composed of two lipped channels of unequal size and a built-up beam composed of two back-to-back lipped channels of equal size. The paper studies the ability of the technique to accurately assess the buckling behaviour of various types of built-up members, including the impact of discrete fasteners. Overall, this research highlights the practical value and wide-ranging applicability of the developed buckling mode decomposition method, providing a valuable tool for the structural analysis and design of built-up members.

1. Introduction

Cold-formed steel (CFS) sections are widely utilised in structural applications due to their high strength-to-weight ratio and ease of integration with other construction materials, making them a versatile choice in modern construction. These sections are commonly used in roofing, wall framing, and low-rise building structures. By connecting multiple individual sections to form a built-up cross-section, CFS members can be extended to mid-rise construction, offering enhanced load-bearing capacity and structural efficiency. Despite their advantages, CFS members are highly susceptible to buckling instabilities, including local and distortional buckling, as well as interactions with global buckling modes, such as flexural and flexural-torsional buckling. Therefore, accurately assessing their structural capacity requires a comprehensive analysis of their buckling behaviour, including the identification of critical buckling modes and corresponding loads.

The challenge of buckling analysis increases with geometric complexity, as intricate cross-sections make it difficult to determine minimum buckling loads for critical modes, particularly when using conventional signature curve analysis based on the finite strip method (FSM). For built-up

[1] Senior Lecturer, The University of Sydney, <mani.khezri@sydeny.edu.au>
[2] Professor, The University of Sydney, <kim.rasmussen@sydeny.edu.au>

members, the problem is further complicated by the presence of discrete fasteners, which can significantly modify the local, distortional, and global buckling response. To effectively analyse and interpret the complex instability behaviour of thin-walled built-up structures, decomposition and superposition techniques are required. These methods involve decomposing the buckled shape into fundamental "basic" modes, which govern the overall failure load and stability behaviour. By identifying and separating these dominant deformation modes, a more precise understanding of buckling interactions in built-up members can be achieved.

Significant progress has been made in the development of numerical methods for the buckling analysis of thin-walled structures, enabling the identification and decomposition of dominant buckling modes. Several established techniques, including Generalized Beam Theory (GBT) (Dinis, Camotim, and Silvestre 2006; Gonçalves, Ritto-Corrêa, and Camotim 2010), the Constrained Finite Strip Method (cFSM) (Ádány and Schafer 2008; Rendall, Hancock, and Rasmussen 2017), and the Constrained Finite Element Method (cFEM) (Ádány 2018; Ádány, Visy, and Nagy 2018), have been instrumental in advancing our understanding of the buckling behaviour of thin-walled members. More recent decomposition methods have been developed for thin-walled structures. The Equivalent Nodal Force (ENF) technique by Becque et al. (Becque, Li, and Davison 2019) decomposes instability patterns based on force equilibrium rather than strain constraints. Hybrid GBT-shell formulations (Habtemariam et al. 2022) enhance accuracy and efficiency in modal analysis. The force/displacement-based fFSM (Jin et al. 2021) extends decomposition to closed and curved sections, addressing limitations of the traditional cFSM. More recently, the Modal Finite Strip Method (mFSM) (Khezri and Rasmussen 2019b, 2019a) has been introduced, offering a strain energy-based decomposition approach that provides a flexible and physically meaningful classification of buckling modes.

While these methods have been successfully applied to single-section thin-walled members, few methods have been extended to built-up members. The presence of discrete fasteners in built-up configurations introduces additional complexities, fundamentally altering the interaction between buckling modes. As a result, conventional modal decomposition techniques, including GBT, cFSM, and cFEM, do not inherently account for the influence of fasteners, and require modifications to be applicable to built-up sections. The generalised beam theory was recently extended (Basaglia, Camotim, and Gonçalves 2024) to analyse the buckling behaviour of cold-formed steel (CFS) built-up members with discrete fasteners by introducing constraint equations to enforce displacement and rotation compatibility at fastener locations. The authors of the present paper developed a comprehensive mFSM decomposition framework for built-up sections (Khezri and Rasmussen 2023), incorporating the effects of discrete fasteners on the local, distortional, and global buckling modes. The proposed methodology builds on the authors' previous work on the Compound Strip Method (CSM) (Abbasi et al. 2018; Khezri, Abbasi, and Rasmussen 2017b; Abbasi, Khezri, and Rasmussen 2017), which was introduced for the finite strip analysis of built-up sections. By integrating mFSM with CSM, a complete decomposition technique is developed that allows for the accurate identification of fundamental buckling modes in built-up sections, including the influence of discrete fasteners on the overall buckling response. This novel framework provides an efficient and scalable approach for analysing the buckling behaviour of complex built-up cold-formed steel members.

The structure of this paper is as follows: Section 2 provides a brief review of the semi-analytical finite strip method (FSM) and its application to the buckling analysis of thin-walled prismatic members. Section 3 introduces the compound strip method (CSM) and its role in modelling discrete fasteners in built-up sections. Section 4 presents the proposed modal decomposition method (mFSM), detailing the necessary modifications for its application to built-up sections. Finally, Section 5 includes two numerical examples to validate the accuracy and effectiveness of mFSM in capturing the modal behaviour of built-up thin-walled columns and beams.

2. Finite strip buckling analysis

2.1 The semi-analytical finite strip method

The finite strip method (FSM) discretises a thin-walled member into *ns* strips along its transverse direction, defined by *n* nodal lines, as illustrated in Figure 1. Longitudinal displacements are represented using analytical functions, such as beam eigenfunctions (Cheung and Cheung 1971) or trigonometric functions (Bradford and Azhari 1995), while polynomial shape functions are employed in the transverse direction. The displacement field at an arbitrary point (x,y) on the mid-surface of a strip (as shown in Figure 1) is expressed as:

$$\begin{aligned} u_s(x,y) &= \sum_{\alpha=1}^{P}\left(\psi_{mu}(x)\mathbf{d}^s_{m\alpha}\right)S_\alpha(y), \\ v_s(x,y) &= \sum_{\alpha=1}^{P}\left(\psi_{mv}(x)\mathbf{d}^s_{m\alpha}\right)\tfrac{L}{\mu_\alpha}S_{\alpha,y}(y), \\ w_s(x,y) &= \sum_{\alpha=1}^{P}\left(\psi_{b}(x)\mathbf{d}^s_{b\alpha}\right)S_\alpha(y), \end{aligned} \tag{1}$$

where P represents the number of terms in the longitudinal direction, S_α denotes the α-th term of the harmonic function series, and μ_α is the corresponding coefficient. The vectors $\mathbf{d}^s{}_{m\alpha}$ and $\mathbf{d}^s{}_{b\alpha}$ define the degrees of freedom (DOFs) associated with membrane and bending displacements, respectively.

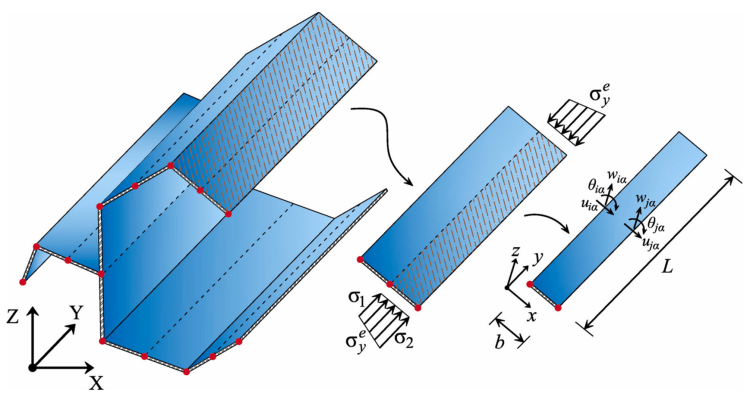

Figure 1: Strip discretization and DOFs, local and global coordinates systems, and nomenclature.

2.2 Internal elastic strain energy and strip stiffness matrices

The flat strip shown in Figure 1 is assumed to maintain its flatness in the presence of applied stresses until it reaches the point of buckling. The strip total strain energy is defined as follows:

$$U^s = \frac{1}{2}\int_V \left(\boldsymbol{\sigma}^s\right)^{\mathrm{T}} \boldsymbol{\varepsilon}^s \mathrm{d}V, \tag{2}$$

which can be decomposed into membrane and bending strain energy components:

$$U^s = \underbrace{\sum_{\alpha=1}^{P}\sum_{\beta=1}^{P}\frac{1}{2}\left(\mathbf{d}^s_{m\alpha}\right)^{\mathrm{T}} \mathbf{k}^s_{m\alpha\beta}\,\mathbf{d}^s_{m\beta}}_{U^s_m} + \underbrace{\sum_{\alpha=1}^{P}\sum_{\beta=1}^{P}\frac{1}{2}\left(\mathbf{d}^s_{b\alpha}\right)^{\mathrm{T}} \mathbf{k}^s_{b\alpha\beta}\,\mathbf{d}^s_{b\beta}}_{U^s_b}, \tag{3}$$

where $\mathbf{k}^s{}_{m\alpha\beta}$ and $\mathbf{k}^s{}_{b\alpha\beta}$ represent the membrane and flexural stiffness matrices of the strip, respectively, and are defined as:

$$\mathbf{k}^s_{m\alpha\beta} = \int_L\int_b \left(\mathbf{B}^s_{m\alpha}\right)^T \mathbf{D}_m \mathbf{B}^s_{m\alpha} t \,\mathrm{d}x\,\mathrm{d}y, \quad \mathbf{k}^s_{b\alpha\beta} = \int_L\int_b \left(\mathbf{B}^s_{b\alpha}\right)^T \mathbf{D}_b \mathbf{B}^s_{b\alpha} \,\mathrm{d}x\,\mathrm{d}y. \tag{4}$$

In Eq. (4), $\mathbf{D}_m$ and $\mathbf{D}_b$ represent the membrane and bending property matrices, respectively, while $\mathbf{B}^s{}_{m\alpha}$ and $\mathbf{B}^s{}_{b\alpha}$ denote the membrane and bending strain compliance matrices (Cheung and Cheung 1971). Using Eq. (4), the strip stiffness matrix corresponding to the half-waves α and β is obtained by assembling the membrane and bending components:

$$\mathbf{k}^s_{\alpha\beta} = \begin{bmatrix} \mathbf{k}^s_{m\alpha\beta} & 0 \\ 0 & \mathbf{k}^s_{b\alpha\beta} \end{bmatrix}. \tag{5}$$

Thus, the total strain energy of the strip can be expressed as:

$$U^s = \sum_{\alpha=1}^{P}\sum_{\beta=1}^{P}\frac{1}{2}\left(\mathbf{d}^s_{\alpha}\right)^{\mathrm{T}} \mathbf{k}^s_{\alpha\beta}\,\mathbf{d}^s_{\beta} = \frac{1}{2}\left(\mathbf{d}^s\right)^{\mathrm{T}} \mathbf{k}^s\,\mathbf{d}^s, \text{ where } \mathbf{k}^s = \begin{bmatrix} \mathbf{k}^s_{11} & \cdots & \mathbf{k}^s_{1P} \\ \vdots & \ddots & \vdots \\ \mathbf{k}^s_{P1} & \cdots & \mathbf{k}^s_{PP} \end{bmatrix}, \text{and } \mathbf{d}^s = \begin{Bmatrix} \mathbf{d}^s_1 \\ \vdots \\ \mathbf{d}^s_P \end{Bmatrix}. \tag{6}$$

2.3 Potential energy of external loads and strip stability matrices

The reduction in potential energy due to in-plane stresses $\boldsymbol{\sigma}^e{}_m$ resulting from the buckling deformation of a flat strip is given by:

$$V^s = \int_V \boldsymbol{\varepsilon}^T_{NL} \boldsymbol{\sigma}^e_m \mathrm{d}V, \tag{7}$$

where $\boldsymbol{\varepsilon}_{NL}$ represents the nonlinear component of the membrane strain vector, defined as (Plank and Wittrick 1974):

$$\boldsymbol{\varepsilon}_{NL} = \left\{ \tfrac{1}{2}\left(\tfrac{\partial w}{\partial x}\right)^2, \tfrac{1}{2}\left(\tfrac{\partial u}{\partial y}\right)^2 + \tfrac{1}{2}\left(\tfrac{\partial v}{\partial y}\right)^2 + \tfrac{1}{2}\left(\tfrac{\partial w}{\partial y}\right)^2, \left(\tfrac{\partial w}{\partial x}\right)\left(\tfrac{\partial w}{\partial y}\right) \right\}^{\mathrm{T}}. \tag{8}$$

Considering only strips subjected to longitudinal in-plane stresses, Eq. (7) can be rewritten as:

$$V^s = \int_V \tfrac{1}{2}\left[\left(\frac{\partial u}{\partial y}\right)^2 + \left(\frac{\partial v}{\partial y}\right)^2\right]\sigma_y^e \,\mathrm{d}V + \int_V \tfrac{1}{2}\left(\frac{\partial w}{\partial y}\right)^2 \sigma_y^e \,\mathrm{d}V. \tag{9}$$

By substituting the general displacement functions from Eq. (1) and performing the appropriate differentiation, one obtains:

$$V^s = \sum_{\alpha=1}^{P}\sum_{\beta=1}^{P} \tfrac{1}{2}(\mathbf{d}_{m\alpha}^s)^{\mathrm{T}} \overbrace{(\int_L\int_b \sigma_y^e (\mathbf{G}_{m\alpha}^s)^{\mathrm{T}} \mathbf{G}_{m\beta}^s t\mathrm{d}x\mathrm{d}y)}^{\mathbf{g}_{m\alpha\beta}^s} \mathbf{d}_{m\beta}^s + \tfrac{1}{2}(\mathbf{d}_{b\alpha}^s)^{\mathrm{T}} \overbrace{(\int_L\int_b \sigma_y^e (\mathbf{G}_{b\alpha}^s)^{\mathrm{T}} \mathbf{G}_{b\beta}^s t\mathrm{d}x\mathrm{d}y)}^{\mathbf{g}_{b\alpha\beta}^s} \mathbf{d}_{b\beta}^s, \tag{10}$$

where $\mathbf{g}^s_{m\alpha\beta}$ and $\mathbf{g}^s_{b\alpha\beta}$ represent the strip membrane and bending stability matrices, respectively, corresponding to the α-th and β-th terms. Similar to the stiffness matrix, the strip stability matrix for the α-th and β-th terms is defined as:

$$\mathbf{g}_{\alpha\beta}^s = \begin{bmatrix} \mathbf{g}_{m\alpha\beta}^s & 0 \\ 0 & \mathbf{g}_{b\alpha\beta}^s \end{bmatrix}. \tag{11}$$

Using the strip stability matrix, the potential energy of the externally applied loads can be expressed as:

$$V^s = \sum_{\alpha=1}^{P}\sum_{\beta=1}^{P} \frac{1}{2}\left(\mathbf{d}_\alpha^s\right)^{\mathrm{T}} \mathbf{g}_{\alpha\beta}^s \,\mathbf{d}_\beta^s = \frac{1}{2}\left(\mathbf{d}^s\right)^{\mathrm{T}} \mathbf{g}^s \,\mathbf{d}^s, \text{ where } \mathbf{g}^s = \begin{bmatrix} \mathbf{g}_{11}^s & \cdots & \mathbf{g}_{1P}^s \\ \vdots & \ddots & \vdots \\ \mathbf{g}_{P1}^s & \cdots & \mathbf{g}_{PP}^s \end{bmatrix}. \tag{12}$$

2.4 Global stiffness and stability matrices

The strip stiffness and stability matrices, derived in Eqs. (6) and (12), are formulated in the local coordinate system assigned to each strip. To construct the global stiffness (**K**) and stability (**G**) matrices for a member composed of multiple strips (Figure 1), these local matrices must be transformed into the global coordinate system and assembled according to the connectivity of the strips. Similarly, the local strip displacement vectors $\mathbf{d}_S$ must be transformed and assembled into the global displacement vector **d**.

2.5 Buckling equation

The total potential energy (Π) consists of the internal elastic strain energy (U) and the reduction in potential energy due to the work of external actions (V):

$$\Pi = U - V. \tag{13}$$

Expressed in terms of the assembled global stiffness (**K**) and stability (**G**) matrices, the internal strain energy and the potential energy due to the work of external loads are given by:

$$U = \tfrac{1}{2}\mathbf{d}^{\mathrm{T}}\mathbf{K}\mathbf{d}, \quad V = \tfrac{1}{2}\mathbf{d}^{\mathrm{T}}\mathbf{G}\,\mathbf{d}. \tag{14}$$

Substituting Eq. (14) into Eq. (13) yields the total potential energy expression for the thin-walled member:

$$\Pi = \tfrac{1}{2}\mathbf{d}^{\mathrm{T}}\mathbf{K}\mathbf{d} - \tfrac{1}{2}\mathbf{d}^{\mathrm{T}}\mathbf{G}\,\mathbf{d} = \tfrac{1}{2}\mathbf{d}^{\mathrm{T}}\left(\mathbf{K} - \lambda\mathbf{G}_u\right)\mathbf{d}, \tag{15}$$

where λ is the load factor that scales the reference stability matrix ($\mathbf{G}_u$) to the actual stability matrix ($\mathbf{G}$) under applied external loads. Minimising the total potential energy in Eq. (15) with respect to $\mathbf{d}$ leads to the buckling eigenvalue equation:

$$\left(\mathbf{K} - \mathbf{\Lambda}\mathbf{G}_u\right)\mathbf{\Phi} = \mathbf{0}, \tag{16}$$

where $\mathbf{\Lambda}$ is the diagonal matrix containing the eigenvalues, and $\mathbf{\Phi}$ is the corresponding eigenmode matrix.

3. Compound strip method for the analysis of built-up sections

A framework for analysing built-up sections with discrete fasteners was introduced by the authors (Abbasi et al. 2018; Khezri, Abbasi, and Rasmussen 2017a), see Figure 2(a). Fasteners are modelled as 3D beam elements with six DOFs per node (Figure 2(b)), providing a flexible numerical tool for parametric studies and structural design.

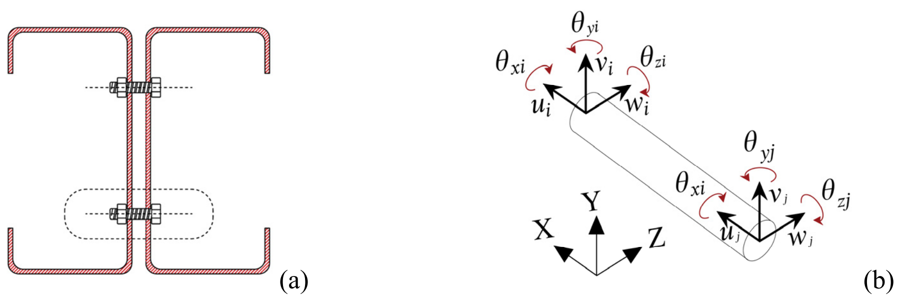

Figure 2. (a) Schematic view of a built-up section with discrete fasteners, (b) local coordinates and degrees of freedom of an arbitrarily oriented connection element.

The force-displacement relationship for a fastener in its local coordinate system is given by:

$$\begin{Bmatrix} \mathbf{F}_i \\ \mathbf{F}_j \end{Bmatrix} = \begin{bmatrix} \mathbf{K}_{ii} & \mathbf{K}_{ij} \\ \mathbf{K}_{ji} & \mathbf{K}_{jj} \end{bmatrix} \begin{Bmatrix} \boldsymbol{\delta}_i \\ \boldsymbol{\delta}_j \end{Bmatrix} = \mathbf{K}_c \boldsymbol{\delta}_c, \tag{17}$$

where:

$$\boldsymbol{\delta}_\mu = \left\{ u_\mu \quad v_\mu \quad w_\mu \quad \theta_{x\mu} \quad \theta_{y\mu} \quad \theta_{z\mu} \right\}^T, \quad \mathbf{F}_\mu = \left\{ F_{x\mu} \quad F_{y\mu} \quad F_{z\mu} \quad M_{x\mu} \quad M_{y\mu} \quad M_{z\mu} \right\}^T, (\mu = i, j) \tag{18}$$

$\mathbf{K}_c$ represents the stiffness matrix of the connection element. The stiffness matrix subcomponents are formulated using in-plane stiffness constants, with detailed derivations available in (Abbasi et al. 2018) for Euler-Bernoulli and Timoshenko beam models. The compound finite strip model incorporates the connection element stiffness while maintaining displacement and rotational compatibility. The system consists of two parallel strips linked by an arbitrarily oriented connection element (see Figure 3).

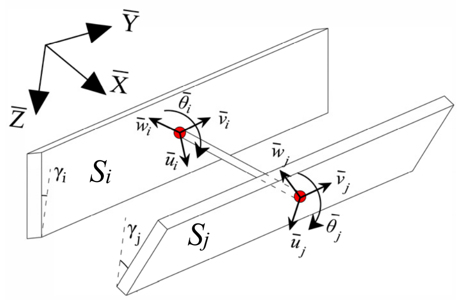

Figure 3. Three-dimensional model for connection element and adjoining constituent strips.

The total strain energy of the considered system is expressed as:

$$\Pi = \Pi_{S_i} + \Pi_{S_j} + \sum_{k=1}^{NC} \Pi_{C_k} \tag{19}$$

where Π_{Si} and Π_{Sj} are the strain energies of the connected strips, NC is the number of connection elements, and Π_{Ck} represents the strain energy of the k-th connection element:

$$\Pi_{C_k} = \tfrac{1}{2} \boldsymbol{\delta}_c^T \mathbf{K}_c \boldsymbol{\delta}_c \tag{20}$$

The displacement field of the connection element is transformed into global nodal displacements using matrices $\mathbf{R}$ and $\mathbf{R}_{GL}$, obtained via single-axis rotations (Chen, Gutkowski, and Puckett 1991; Wiseman and Puckett 1991). The components of $\mathbf{R}_{GL}$ depend on the orientation angles (γ_i, γ_j) of the connected strips (Figure 3), as detailed in (Abbasi et al. 2018). Interpolation matrices $\boldsymbol{\psi}^m_\mu$ and $\boldsymbol{\psi}^n_\mu$ ($\mu = i, j$) relate the displacement field of the connection element to that of the strips. The process is summarised as:

$$\bar{\mathbf{K}}_c^{nm} = \mathbf{R}_{GL} \left(\boldsymbol{\psi}^n\right)^{\mathrm{T}} \left(\mathbf{R}_{GL}\right)^{\mathrm{T}} \mathbf{R}^{\mathrm{T}} \mathbf{K}_c \, \mathbf{R} \, \mathbf{R}_{GL} \, \boldsymbol{\psi}^m \left(\mathbf{R}_{GL}\right)^{\mathrm{T}} \tag{21}$$

The stiffness contributions of the connection elements are incorporated into the system matrix while maintaining displacement and rotational compatibility (Abbasi et al. 2018). To facilitate modal decomposition for built-up sections, a separate matrix ($\mathbf{K}_{cnts}$) is introduced to store the stiffness contributions of the connection elements. For a built-up member composed of N single sections, the system stiffness matrix $\mathbf{TK}$ is given by:

$$\left[\mathbf{TK}\right]_{nt\times nt} = \underbrace{\underbrace{\begin{bmatrix} \mathbf{K}_1 & 0 & \cdots & 0 \\ 0 & 0 & \cdots & 0 \\ \vdots & \vdots & \ddots & 0 \\ 0 & 0 & 0 & 0 \end{bmatrix}}_{nt\times nt} + \underbrace{\begin{bmatrix} 0 & 0 & \cdots & 0 \\ 0 & \mathbf{K}_2 & \cdots & 0 \\ \vdots & \vdots & \ddots & 0 \\ 0 & 0 & 0 & 0 \end{bmatrix}}_{nt\times nt} + \dots + \underbrace{\begin{bmatrix} 0 & 0 & \cdots & 0 \\ 0 & 0 & \cdots & 0 \\ \vdots & \vdots & \ddots & 0 \\ 0 & 0 & 0 & \mathbf{K}_N \end{bmatrix}}_{nt\times nt}}_{N} + \left[\mathbf{K}_{cnts}\right]_{nt\times nt} \text{ or } \mathbf{TK} = \mathbf{K} + \mathbf{K}_{cnts} \tag{22}$$

where *nt* is the total number of DOFs.

4. Modal finite strip method (mFSM)

4.1 Theory and background

Modal decomposition methods express arbitrary displacement fields as linear combinations of structurally meaningful "pure" modes, forming an orthogonal basis. The deformation spaces are categorized into global (G), distortional (D), local (L), shear (S), and transverse extension (TE) modes, following the classification framework of (Ádány and Schafer 2014a, 2014b). These classification criteria are summarized in Table 1.

Table 1: Mechanical criteria for mode classes (Ádány and Schafer 2014a, 2014b)

	G			D	L		S									TE	
	G_A	G_B	G_T		L_P	L_S	S_{Bt}	S_{Tt}	S_{Dt}	S_{Ct}	S_{Bw}	S_{Tw}	S_{Dt}	S_{Cw}	S_{Sw}	TE_P	TE_S
$\varepsilon_x = 0$		Y		Y	Y						Y					N	
$\gamma_{xy} = 0$		Y		Y	Y						N					N	
Trans. Eq.		Y		Y	N		Y	Y	Y	N	Y	Y	Y	Y	Y	N	
$\varepsilon_y = 0$		N		N	Y		Y	Y	Y	Y	N	N	N	N	N	Y	
$\kappa_x = 0$		Y		N	N		Y	Y	N	N	Y	Y	Y	Y	Y	N	Y
$\kappa_y = 0$	Y	Y	N	N	N	N	Y	N	N	N	Y	Y	Y	Y	Y	N	Y
$\kappa_{xy} = 0$	Y	N	N	N	N	N	N	N	N	N	Y	Y	Y	Y	Y	N	Y

This study adopts the modal identification and classification framework previously developed for the constrained Finite Strip Method (cFSM) and the mFSM (Khezri and Rasmussen 2019b, 2019a, 2018). In cFSM, constraint matrices ($\mathbf{R}_M$) are introduced to map the general deformation space ($\mathbf{d}$) onto constrained modal spaces ($\mathbf{d}_M$), as:

$$\mathbf{d} = \mathbf{R}_M \mathbf{d}_M \tag{23}$$

where the columns of $\mathbf{R}_M$ define the base vectors for each of the deformation modes. This mapping extends to eigenmodes ($\mathbf{\Phi}$), leading to:

$$\mathbf{\Phi} = \mathbf{R}_M \mathbf{\Phi}_M . \tag{24}$$

which results in the constrained eigenvalue problem:

$$\left(\mathbf{R}_M^T \mathbf{K} \mathbf{R}_M - \mathbf{\Lambda}_M \mathbf{R}_M^T \mathbf{G}_u \mathbf{R}_M \right) \mathbf{\Phi}_M = \mathbf{0}, \quad \text{or in short,} \quad \left(\mathbf{K}_M - \mathbf{\Lambda}_M \mathbf{G}_M \right) \mathbf{\Phi}_M = \mathbf{0}, \tag{25}$$

where $\mathbf{K}$ and $\mathbf{G}_u$ are the global stiffness and stability matrices, while $\mathbf{K}_M$ and $\mathbf{G}_M$ represent their constrained counterparts.

Unlike cFSM, mFSM constructs modal base vectors by solving a generalised eigenvalue problem, determining the strain energy ratio for each mode (Khezri and Rasmussen 2019b, 2019a, 2018):

$$\Upsilon_M = \frac{\mathbf{H}_M^T \mathbf{K}_M \mathbf{H}_M}{\mathbf{H}_M^T \mathbf{K} \mathbf{H}_M}, \tag{26}$$

where $\mathbf{H}_M$ represents the modal base vectors, and $\mathbf{K}_M$ is the modal stiffness matrix, formulated based on the kinematic constraints of mode M. Additional constraints, such as transverse equilibrium and mode orthogonality, are enforced by modifying $\mathbf{H}_M$. To obtain the strain energy ratios required in Eq. (26), the following generalised eigenvalue problem must be solved:

$$\left(\left(\mathbf{H}_M^{\mathrm{T}} \mathbf{K}_M \mathbf{H}_M\right) - \Upsilon_M \left(\mathbf{H}_M^{\mathrm{T}} \mathbf{K} \mathbf{H}_M\right)\right) \boldsymbol{\Theta}_M = \mathbf{0}. \tag{27}$$

The eigenmode matrix $\boldsymbol{\Theta}_M$ is obtained from this eigenvalue problem, and the constraint matrix $\mathbf{R}_M$ is extracted by selecting eigenvectors that satisfy the required modal conditions.

4.2 Extension to Built-Up Sections

For a built-up member consisting of N single sections, the mFSM framework developed for individual sections (Khezri and Rasmussen 2019a, 2019b, 2018) has been extended to built-up members in (Khezri and Rasmussen 2023). This extension involves assembling the built-up members stiffness submatrices associated with each strain component as block-diagonal matrices. For example, the stiffness sub-matrix corresponding to the axial strain ε_x is given by:

$$\left[\mathbf{K}_{\varepsilon_x}\right] = \begin{bmatrix} \mathbf{K}_{\varepsilon_x}^1 & \cdots & 0 \\ \vdots & \ddots & \vdots \\ 0 & \cdots & \mathbf{K}_{\varepsilon_x}^N \end{bmatrix}, \tag{28}$$

where $\mathbf{K}_{\varepsilon_x}^i$ represents the contribution of the i-th single section. The same formulation applies to other strain components $\left(\mathbf{K}_{\varepsilon_y}, \mathbf{K}_{\varepsilon_x\varepsilon_y}, \mathbf{K}_{\gamma_{xy}}, \mathbf{K}_{\kappa_x}, \mathbf{K}_{\kappa_y}, \mathbf{K}_{\kappa_x\kappa_y}, \mathbf{K}_{\kappa_{xy}}\right)$, each with a corresponding stiffness matrix structured in a similar block-diagonal form. These stiffness submatrices for the built-up sections are used to determine the appropriate $\mathbf{K}_M$ matrices for the mode (M) in question. The key modifications for built-up members involve:

(1) Aggregating the stiffness contributions from all sections while excluding fastener stiffness terms in the modal stiffness matrix $\mathbf{K}_\mathrm{M}$
(2) Replacing the single-section stiffness matrix $\mathbf{K}$ with the system stiffness matrix $\mathbf{TK}$, which includes fastener stiffness contributions via Eq. (22).

Thus, the ratio of the elastic strain energy developed under mode M deformations to that of general displacements for a built-up member can be derived as:

$$\Upsilon_M = \frac{\mathbf{H}_M^T \mathbf{K}_M \mathbf{H}_M}{\mathbf{H}_M^T \mathbf{TK} \mathbf{H}_M} = \frac{\mathbf{H}_M^T \mathbf{K}_M \mathbf{H}_M}{\mathbf{H}_M^T (\mathbf{K} + \mathbf{K}_{cnts}) \mathbf{H}_M}. \tag{29}$$

where $\mathbf{TK}$ is the system stiffness matrix incorporating the fastener stiffness matrix $\mathbf{K}_{cnts}$, ensuring compatibility with the fastener-influenced buckling behaviour. The procedure for extracting pure modes follows the approach described in (Khezri and Rasmussen 2019a, 2019b, 2018) and its extension to built-up members in (Khezri and Rasmussen 2023). The initial $\mathbf{H}_M$ matrix for the global axial mode (G_A) is chosen as the range of the eigenmodes matrix $\mathbf{\Phi}$, computed via singular value decomposition (SVD) (Strang 1993). This ensures that the decomposition is performed in a space that is compatible with the deformation modes of the built-up member. Finally, to maintain consistency with Generalized Beam Theory (GBT) assumptions, Poisson's effects are ignored by setting $\nu = 0$, thus eliminating strain interaction terms (Ádány et al. 2009).

5. Numerical examples

5.1 General

In this section, we investigate the applicability of the proposed modal Finite Strip Method (mFSM) for analysing the buckling behaviour of built-up sections through two numerical examples. The study begins by evaluating the buckling response of the individual constituent sections to establish a baseline understanding of their structural behaviour. Subsequently, the Compound Strip Method (CSM) is employed to analyse the buckling characteristics of the built-up section formed by combining these individual components. Following this, the mFSM is applied to perform a modal decomposition of the buckling deformations for both the single and built-up sections, providing a deeper insight into their stability characteristics. To ensure the reliability of the results, finite element (FE) solutions obtained using ABAQUS are included for validation where applicable.

5.2 Example 1: Built-up column with back-to-back C-sections of different profiles

This example investigates the buckling behaviour of a built-up column composed of back-to-back C-sections with different size profiles. The section profiles used in this study are shown in Figure 4(a). The sections have different dimensions but are selected to exhibit similar local and distortional buckling loads. The finite strip (FS) discretisation utilised for the analysis is presented in Figure 4(b). A 30 mm fastener spacing is selected to ensure that a sufficient number of built-up sections can be analyzed, particularly for shorter columns. The first row of fasteners is placed 5 mm from each end, resulting in column lengths of 40 mm, 70 mm, 100 mm, 130 mm, and so on. If a larger spacing, such as 50 mm, were used, the column lengths would instead be 60 mm, 110 mm, 160 mm, reducing the total number of columns analysed. To validate the results, a finite element (FE) analysis is performed in ABAQUS, incorporating the same section profiles and fastener spacing. This allows for a comprehensive comparison between FS and FE predictions of buckling behaviour.

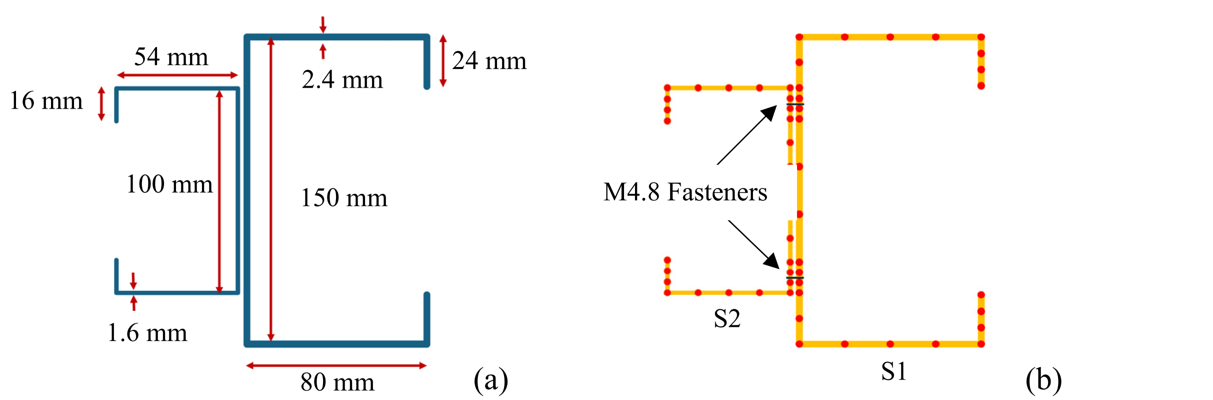

Figure 4: (a) Cross-sectional dimensions of the two different C-sections used in the built-up column configuration. (b) Finite Strip (FS) discretization of the back-to-back built-up column, showing the fastener locations

Signature Curves and Modal Decomposition of Individual Sections

The first step in the analysis is obtaining the signature curves of the individual sections (S1 and S2) under pin-ended boundary conditions. The buckling behaviour is analysed over a length range of 30 mm to 7,000 mm, considering only a single longitudinal term ($m = 1$). The resulting signature curves are presented in Figure 5. To further investigate the buckling characteristics, the modal Finite Strip Method (mFSM) is employed to decompose the signature curves into pure local, distortional, and global buckling modes. The decomposed results for S1 and S2 are also shown in Figure 5. As observed, both sections exhibit similar local and distortional buckling minima values, but these critical loads occur at different lengths. The corresponding buckling mode shapes at the local and distortional minima are illustrated in Figure 5, along with the global flexural-torsional buckling mode at 1585 mm.

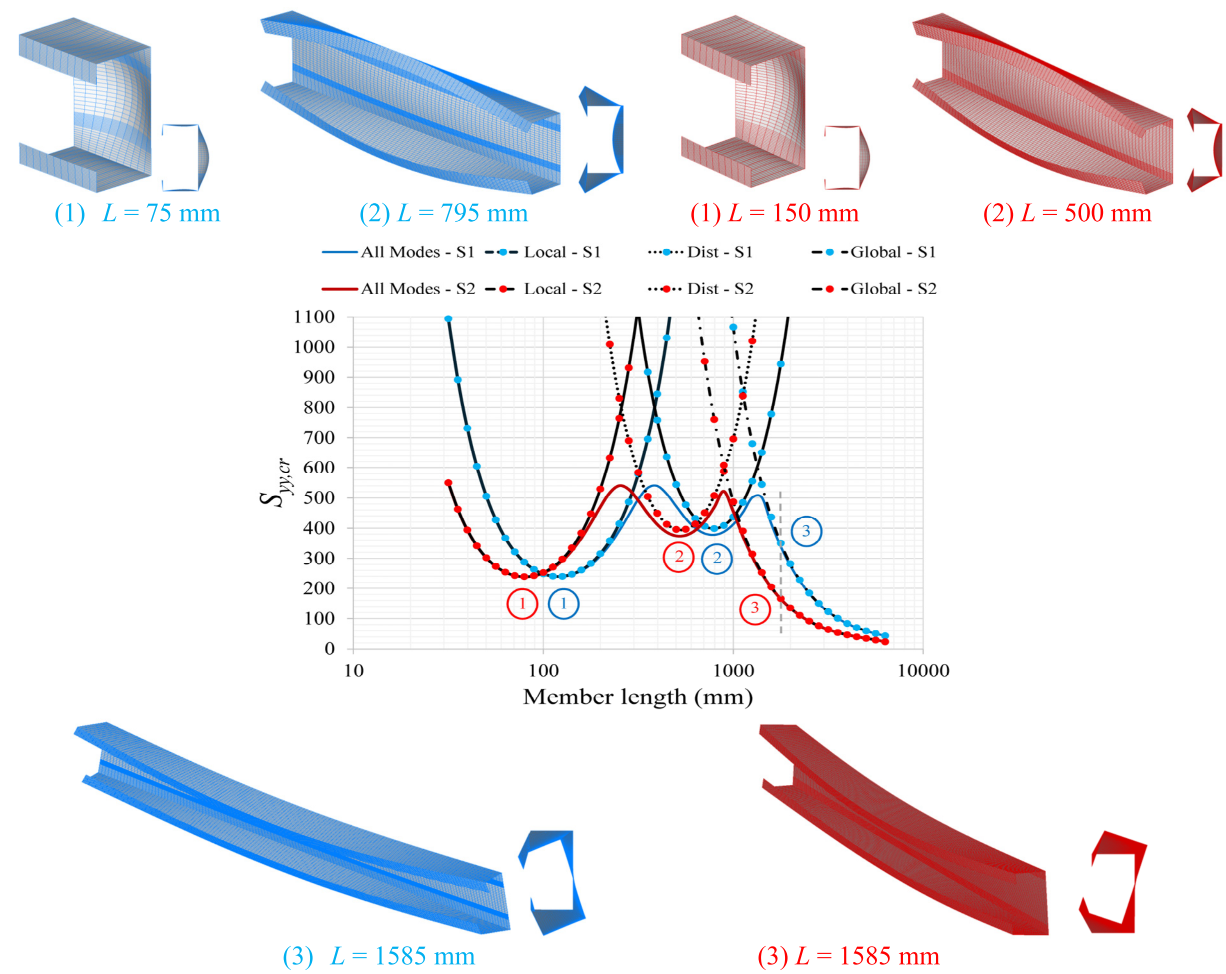

Figure 5. Signature curves of sections S1 and S2, showing buckling behaviour with pure local, distortional, and global mode decomposition.

Comparison with Finite Element Analysis (FEA)

To validate the FSM results, the S1 and S2 sections are also analysed by Finite Element Analysis (FEA) using ABAQUS. The models utilise S4R shell elements, and a sufficiently fine mesh is employed to ensure convergence. It is well-known that FEA and FSM with a single longitudinal term (m = 1) may yield different results. Difference arise because, in FE models, a large number of elements are used in the longitudinal direction (member length), inherently leading to results that deviate from those obtained using the FSM with a single term. To improve the consistency between FSM and FEA, the number of longitudinal terms in FSM (m_{max}) is increased to accurately capture longitudinal flexibility.

The results obtained using FSM with $m_{\max}$ terms and FEA are compared in Figure 6(a). Additionally, the buckling behaviours of the individual sections (S1 and S2) and the built-up column are analysed using both methods. As expected, the built-up section exhibits significant enhancement in buckling loads, especially for the global mode, but also for the local mode due to the closely spaced fasteners.

Buckling Mode Decomposition of the Built-Up Column

The mFSM is also applied to decompose the all-modes buckling curve obtained using multiple longitudinal terms (m_{max}). Typically, modal decomposition is performed on signature curves with m = 1; however, this example demonstrates the capabilities of mFSM in buckling mode decomposition beyond single-term analysis. The decomposed local, distortional, and global mode curves for the built-up column are presented in Figure 6(b). The results show that:

- Local buckling dominates over a wide range of lengths (40 mm to 2000 mm), closely matching the all-modes curve.
- For lengths exceeding 2000 mm, global buckling becomes progressively dominant, as evidenced by the global mode curve aligning with the all-modes curve at lengths greater than 2000 mm.
- The distortional buckling curve remains consistently above the minimum of the local and global curves, indicating that distortional buckling is not the governing mode in this case.

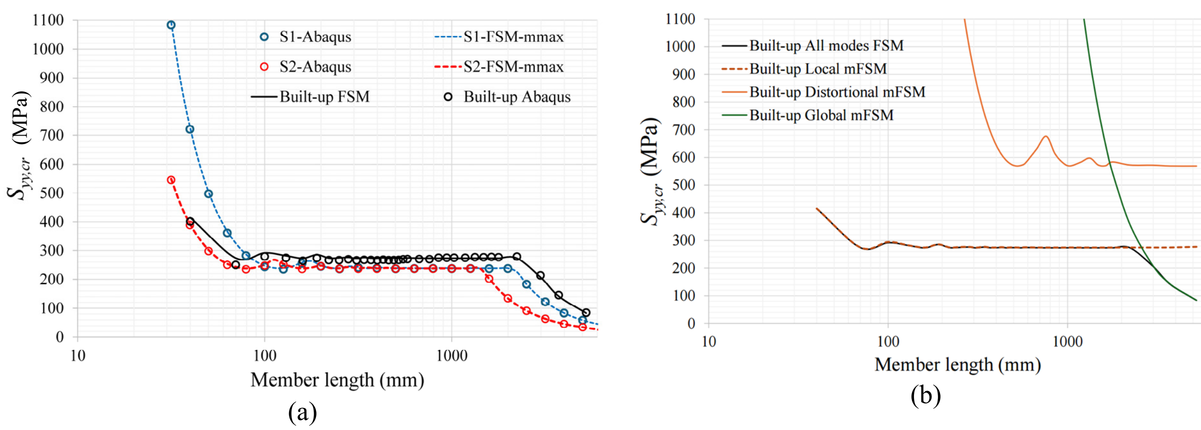

Figure 6. (a) Comparison of buckling loads obtained using FSM with $m_{\max}$ and FEA for S1, S2, and the built-up column (b) Modal decomposition of the built-up column's buckling behaviour using the FSM with $m_{\max}$

Comparison of Buckling Loads

Table 2 presents the buckling stresses at selected member lengths (100, 250, 1030, and 3730 mm) for both the constituent sections (S1 and S2) and the built-up column, along with the ratios between them and the corresponding FEA buckling stresses obtained using Abaqus.

The buckling stress ratios indicate a notable enhancement in buckling capacity due to the composite action between the sections, facilitated by the fasteners. The improvement is particularly pronounced in the global buckling region, where the built-up column exhibits an approximately 50% increase in buckling capacity compared to section S1.

Table 2. Comparison of buckling stresses (MPa) from FSM and FEM for sections S1, S2, and the built-up column

Member length (mm)	Section S1		Section S2		Built-up		Load ratio (FSM)	
	FSM m_{max}	Abaqus	FSM m_{max}	Abaqus	FSM m_{max}	Abaqus	$S_{yy,bu}/S_{yy,S1}$	$S_{yy,bu}/S_{yy,S2}$
100	247.43	243.36	250.55	247.82	291.90	279.39	1.20	1.17
250	238.77	236.27	238.38	236.64	274.64	266.63	1.16	1.15
1030	238.67	237.07	238.28	237.15	273.32	275.26	1.15	1.15
3730	93.653	95.506	50.773	51.552	141.67	145.60	1.48	2.79

The buckling analysis results for the built-up member using the compound strip method with a single longitudinal term (m = 1) are presented in Figure 7. The mFSM decomposition results are also included, showing the pure local, distortional, and global buckling mode curves for the built-up section. The all-modes curve for the built-up (BU) section is consistently higher than the buckling curves of the individual sections (S1 and S2) across all length ranges, confirming the enhanced buckling resistance of the built-up configuration.

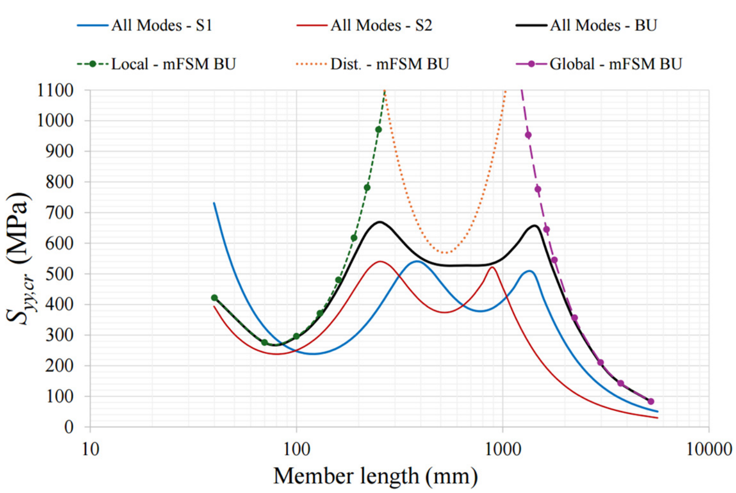

Figure 7. Comparison of buckling curves for the built-up section with those of its constituent sections (S1 and S2)

It is noted that the enhancement in the local region is due to close spacing of fasteners (S = 30), and for larger values of spacing the change in local buckling capacity will be negligible. The greatest improvements occur in the distortional and global buckling regions, particularly at longer column lengths, where the built-up column exhibits a significant increase in buckling capacity. For the built-up member, in the local buckling region (40 mm – 200 mm), the local buckling curve closely follows the all-modes curve, indicating that local buckling governs at shorter column lengths. The distortional buckling minimum obtained using mFSM is higher than the local buckling capacity, further confirming that local buckling is the dominant sectional mode for this built-up section.

The first three pure local, distortional, and global buckling mode shapes, obtained using mFSM for a built-up column of length 250 mm, are shown in Figure 8, Figure 9, and Figure 10, respectively. These results provide further insight into the mechanisms governing the buckling response of the built-up member.

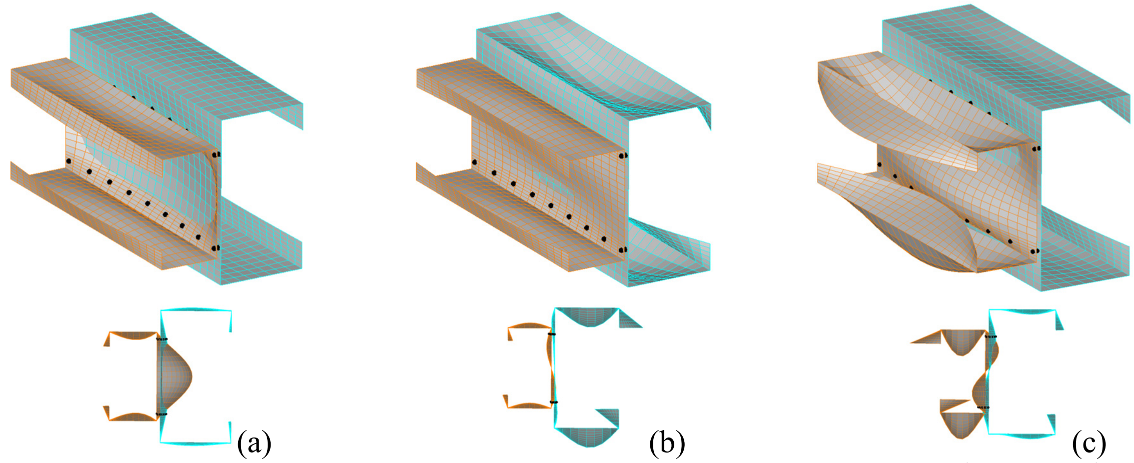

Figure 8. Pure local mode shapes of built-up column at length L= 250 mm (a) 1st (b) 2nd , and (c) 3rd modes

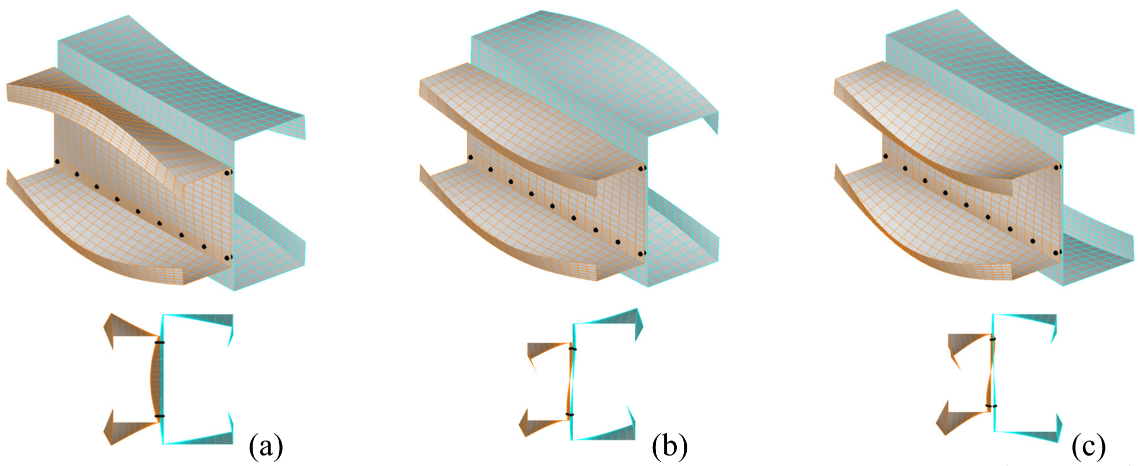

Figure 9. Pure distortional mode shapes of built-up column at length L= 250 mm (a) 1st (b) 2nd, and (c) 3rd modes

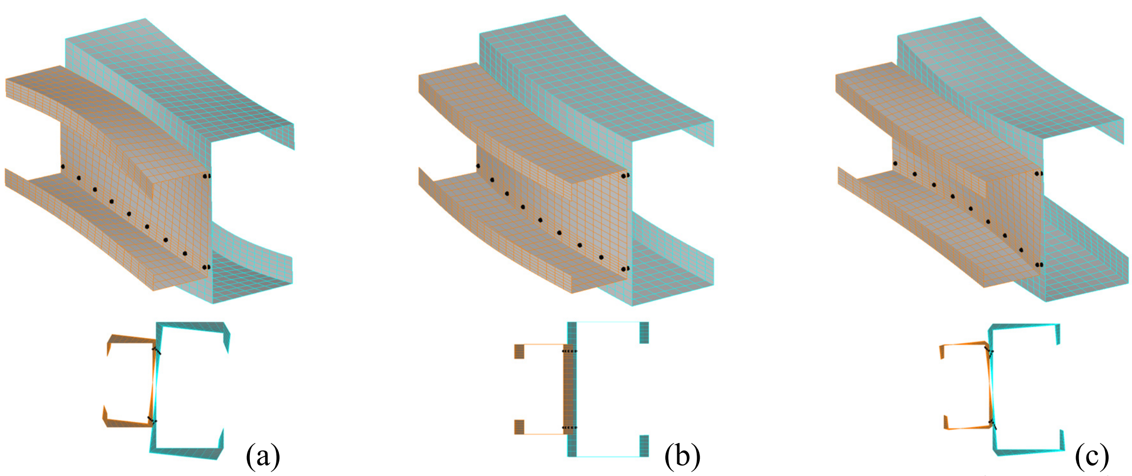

Figure 10. Pure global mode shapes of built-up column at length L= 250 mm (a) 1st (b) 2nd, and (c) 3rd modes

5.2 Example 2: Built-up beam with back-to-back identical C-sections

In this example, two identical lipped C-sections are connected back-to-back using M4.8 fasteners with a longitudinal spacing of 50 mm. The cross-section geometry and dimensions are shown in Figure 11(a), while the finite strip (FS) discretization and fastener locations are illustrated in Figure 11(b). The fastener spacing of 50 mm is chosen to be shorter than the local buckling half-wavelength to allow the fasteners to influence both local and distortional buckling modes. This spacing is smaller than typical fastener spacings used in practice, ensuring a more pronounced interaction between the connected sections. The first row of fasteners is positioned 5 mm from the member ends, resulting in a minimum built-up member length of 60 mm.

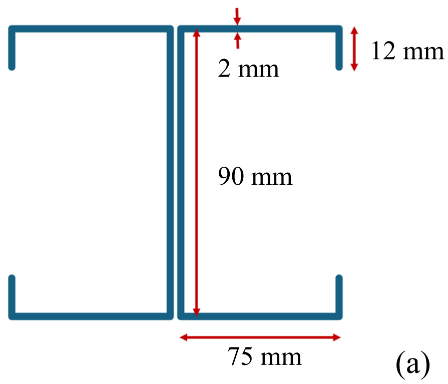

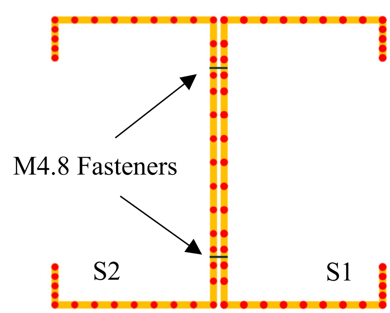

Figure 11: Built-up I-section beam: (a) geometry and dimensions, (b) finite strip discretization and fastener locations

Buckling Analysis of the Constituent Sections Under Pure Bending

The buckling behaviour of a single C-section is first examined under pure bending, where the applied reference bending moment is determined to generate compressive and tensile stresses of magnitude 1 MPa at the extreme fibres (on the flanges). The finite strip (FS) analysis using a single longitudinal term (m = 1) shows that the section is prone to both local and distortional buckling, with two distinct buckling minima:

- Local buckling at L = 70 mm
- Distortional buckling at L = 445 mm

The buckling mode shapes corresponding to these lengths are illustrated in Figure 12, showing the characteristic deformation patterns associated with local and distortional buckling.

The modal Finite Strip Method (mFSM) results for buckling mode decomposition are also presented in Figure 12, depicting the pure local, distortional, and global buckling mode curves. The results confirm that:

(1) The local and distortional buckling mode minima align closely with the minima obtained from the all-modes analysis, validating the decomposition process.
(2) For member lengths exceeding 2500 mm, the global buckling curve coincides with the all-modes curve, indicating that global buckling is the dominant failure mode for longer members.

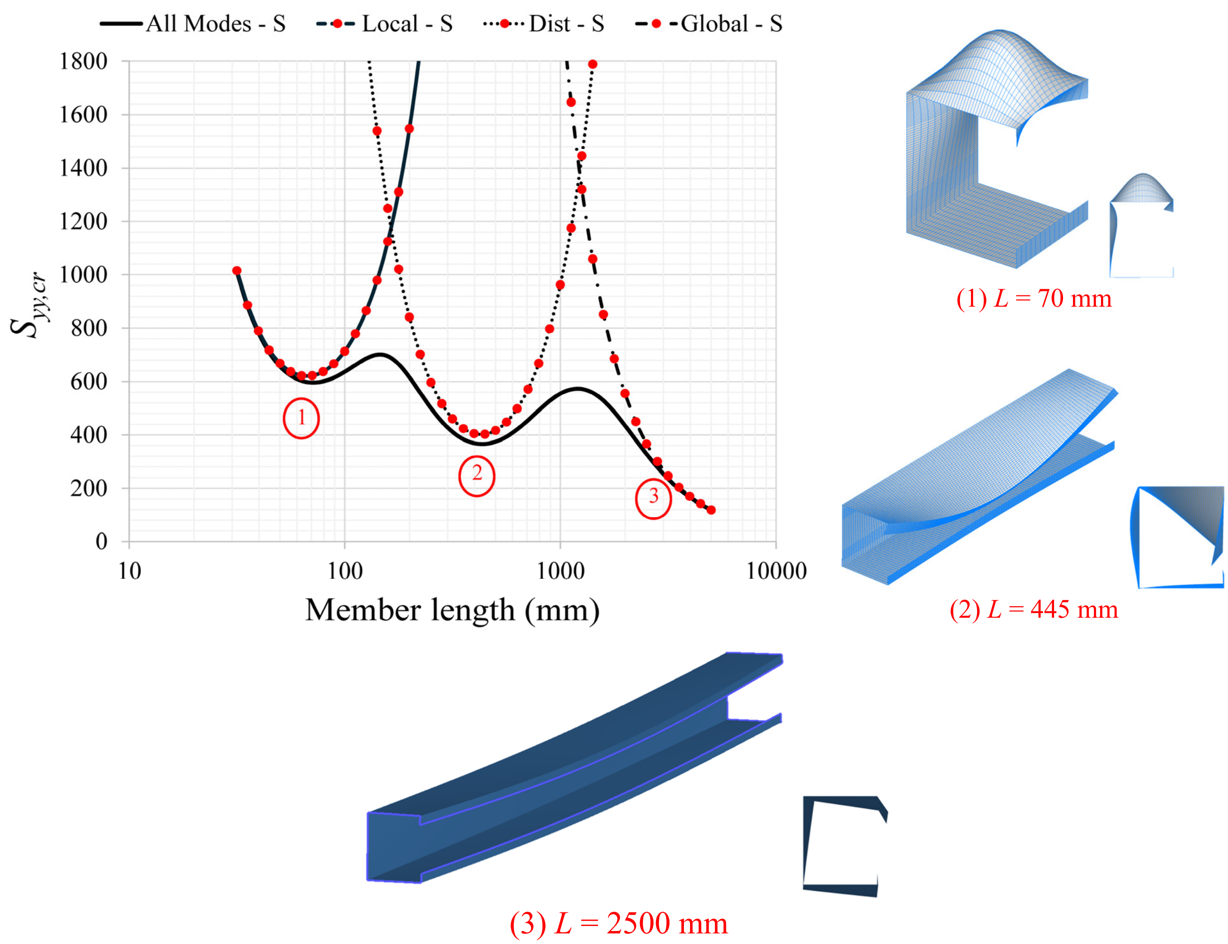

Figure 12. Signature curves of constituent section (S) subjected to pure bending, showing buckling behaviour with pure local, distortional, and global mode decomposition.

The buckling response of the built-up beam member is examined using the compound strip method, with the results presented in Figure 13. For comparison, the all-modes buckling curve for the single-section member is also included. Additionally, the buckling mode shapes at lengths (1) L = 60 mm, (2) L = 410 mm, and (3) L = 2520 mm are provided to illustrate the deformation characteristics of the built-up section.

The local buckling capacity of the built-up member is similar to that of the single-section member, as indicated by the overlap between the buckling curves of the single section and the built-up section in the short-length range. This behaviour is expected partly because a larger fastener spacing of 50 mm is used for the built-up beam member and partly because fasteners generally have limited effect on the local buckling capacity due to its short half-wavelength. A considerable enhancement in buckling capacity is observed in the distortional and global buckling regions, with the built-up section showing higher critical loads compared to the single-section member. This improvement is attributed to the fastener-induced composite action, which increases the overall stiffness and strength of the system.

The mFSM decomposition results, also shown in Figure 13, depict the pure local, distortional, and global buckling mode curves. The results reveal that, (1) the distortional buckling curve is notably higher than the all-modes curve, indicating that while distortional buckling is the primary mode in this range, contributions from other modes also influence the overall buckling response, and (2) the global buckling curve coincides with the all-modes curve for lengths exceeding 2500 mm, demonstrating that global buckling is the dominant mode at long lengths. To further examine the buckling behaviour, the pure mode shapes (mFSM) at selected critical lengths are illustrated:

(1) L = 60 mm: Characterised by short-wavelength deformations primarily affecting the flange and web regions.
(2) L = 410 mm: Displays cross-sectional deformations involving flange rotation and web distortion, which are characteristic of distortional instability.
(3) L = 2560 mm: Exhibits a long-wavelength buckling mode involving overall lateral displacement and twisting of the entire built-up section.

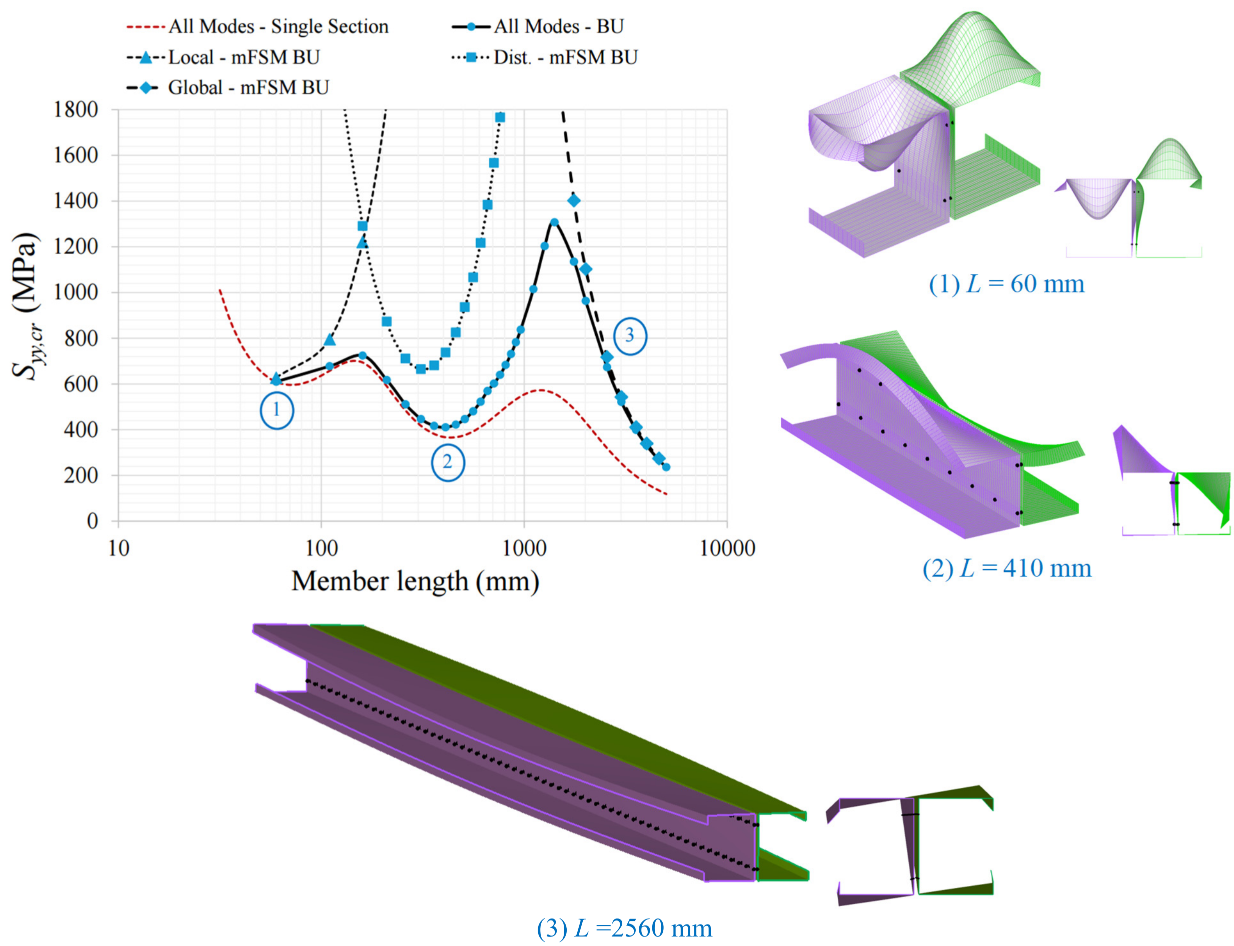

Figure 13. Comparison of buckling curves for the built-up section with its constituent sections and pure buckling mode shapes at (1) L = 60 mm, (2) L = 410 mm, and (3) L = 2520 mm

The pure local, distortional, and global buckling mode shapes for a built-up beam of length 210 mm, obtained using mFSM, are presented in Figure 14, Figure 15, and Figure 16, respectively. For the considered beam, only two meaningful distortional buckling mode shapes exist, as illustrated in Figure 15. Two distinct global buckling mode shapes are observed for the built-up beam and these are depicted in Figure 16, highlighting different global instability mechanisms, including lateral-torsional buckling and flexural buckling.

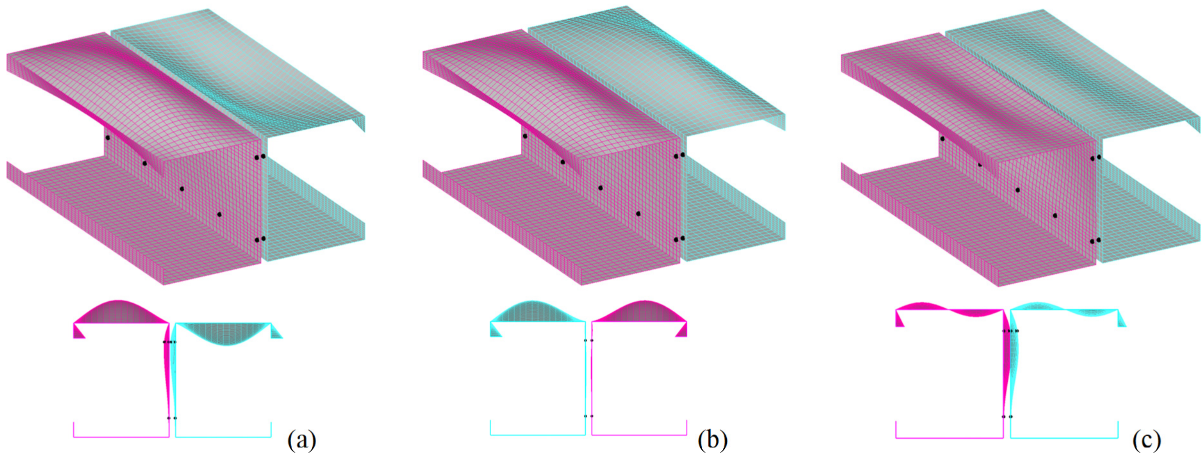

Figure 14. Pure local mode shapes of built-up section beam at length L = 210 mm (a) 1st (b) 2nd, and (c) 3rd modes

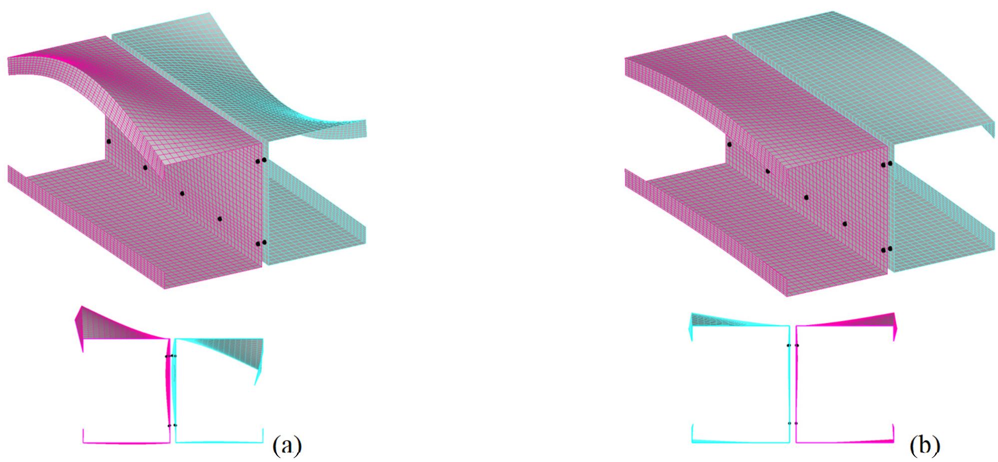

Figure 15. Pure distortional mode shapes of built-up section beam at length L = 210 mm (a) 1st, and (b) 2nd modes

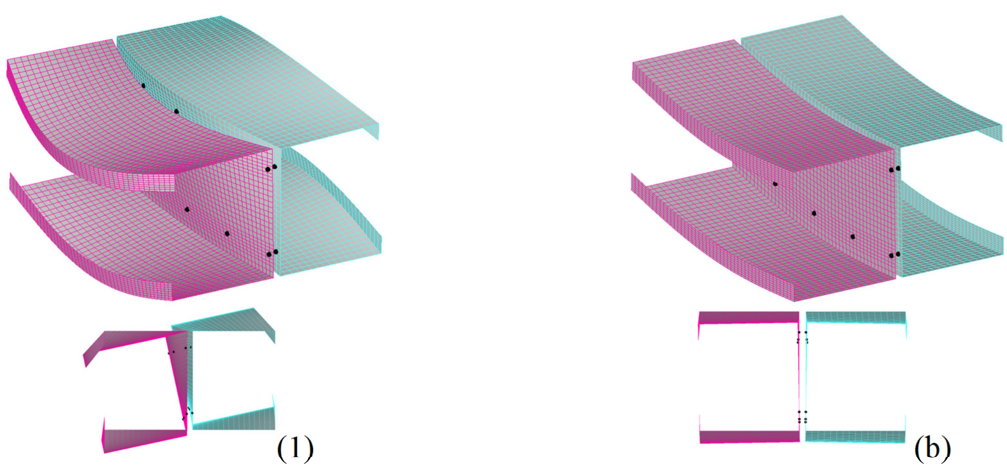

Figure 16. Pure global mode shapes of built-up section beam at length L = 210 mm (a) 1st t, and (b) 2nd modes

As shown in Figure 16, the second pure global mode corresponds to a flexural buckling mode about the major axis of the beam. This buckling mode is not accounted for in existing analytical solutions, such as those provided by (Trahair 2017) for the buckling of beams subjected to bending. Further examination of the buckling loads associated with this mode revealed extremely high buckling stresses, which remained independent of the examined length. These large buckling stresses indicate that, while such a buckling shape may numerically exist, it is not physically feasible for the beam to attain this mode in practice.

6. Conclusions

This study presented the Modal Finite Strip Method (mFSM) for the decomposition of buckling modes of built-up cold-formed steel (CFS) members, demonstrating its effectiveness through two distinct numerical examples of a built-up section column and a built-up section beam. The method, which extends previous work on single-section modal decomposition, was successfully applied to built-up sections by incorporating the effects of discrete fasteners using the Compound Strip Method (CSM) framework.

The results highlight the significant influence of fastener spacing on the interaction between local, distortional, and global buckling modes. While the local buckling behaviour remains largely unchanged, unless a very short fastener spacing is used, the distortional and global buckling capacities are significantly enhanced due to the composite action provided by fasteners. The mFSM decomposition revealed the dominant modal contributions at different length scales, confirming the capability of the mFSM method to accurately separate pure buckling modes and track their evolution in built-up configurations.

Comparison with finite element analysis (FEA) validated the accuracy of the proposed approach, demonstrating that mFSM provides reliable predictions with significantly reduced computational effort compared to full shell-element based modelling. This makes mFSM a practical and efficient tool for the structural analysis and design of built-up CFS members, enabling engineers to better understand buckling behaviour and optimize design parameters.

Acknowledgments

This project was undertaken as a part of Australian Research Council (ARC) Discovery Project DP220103573.

References

Abbasi, M., Khezri, M., and Rasmussen, K. J. R. (2017). 'On extending the direct strength method to the design of cold-formed steel built-up columns.' *ce/papers*, 1(2-3), 1600-1608.

Abbasi, M., Khezri, M., Rasmussen, K. J. R., and Schafer, B. W. (2018). 'Elastic buckling analysis of cold-formed steel built-up sections with discrete fasteners using the compound strip method.' *Thin-Walled Structures*, 124, 58-71.

Ádány, S. (2018). 'Constrained shell Finite Element Method for thin-walled members, Part 1: constraints for a single band of finite elements.' *Thin-Walled Structures*, 128, 43-55.

Ádány, S., and Schafer, B. W. (2008). 'A full modal decomposition of thin-walled, single-branched open cross-section members via the constrained finite strip method.' *Journal of Constructional Steel Research*, 64(1), 12-29.

Ádány, S., and Schafer, B. W. (2014a). 'Generalized constrained finite strip method for thin-walled members with arbitrary cross-section: Primary modes.' *Thin-Walled Structures*, 84, 150-169.

Ádány, S., and Schafer, B. W. (2014b). 'Generalized constrained finite strip method for thin-walled members with arbitrary cross-section: Secondary modes, orthogonality, examples'. *Thin-Walled Structures*, 84, 123-13

Ádány, S., Silvestre, N., Schafer, B. W., and Camotim, D. (2009). 'GBT and cFSM: two modal approaches to the buckling analysis of unbranched thin-walled members.' *Advanced steel construction*, 5(2), 195-223.
Ádány, S., Visy, D., and Nagy, R. (2018). 'Constrained shell Finite Element Method, Part 2: application to linear buckling analysis of thin-walled members'. *Thin-Walled Structures*, 128, 56-70.
Basaglia, C., Camotim, D., and Gonçalves, R. (2024). 'Buckling analysis of cold-formed steel built-up columns using Generalized Beam Theory'. *Proceedings of Structural Stability Research Council (SSRC) 2024 Annual Stability Conference*,
Becque, J., Li, X., and Davison, B. (2019). 'Modal decomposition of coupled instabilities: The method of the equivalent nodal forces.' *Thin-Walled Structures*, 143, 106229.
Bradford, M. A., and Azhari, M. (1995). 'Buckling of plates with different end conditions using the finite strip method.' *Computers & structures*, 56(1), 75-83.
Chen, C. J., Gutkowski, R. M., and Puckett, J. A. (1991). 'B-spline compound strip formulation for braced thin-walled structures.' *Journal of Structural Engineering*, 117(5), 1303-1316.
Cheung, M. S., and Cheung, Y. K. (1971). 'Natural vibrations of thin, flat-walled structures with different boundary conditions.' *Journal of Sound and Vibration*, 18(3), 325-337.
Dinis, P. B., Camotim, D., and Silvestre, N. (2006). 'GBT formulation to analyse the buckling behaviour of thin-walled members with arbitrarily 'branched'open cross-sections.' *Thin-Walled Structures*, 44(1), 20-38.
Gonçalves, R., Ritto-Corrêa, M., and Camotim, D. (2010). 'A new approach to the calculation of cross-section deformation modes in the framework of generalized beam theory.' *Computational Mechanics*, 46, 759-781.
Habtemariam, A. K., Bianco, M. J., Könke, C., and Zabel, V. (2022). 'Geometrically nonlinear formulation of Generalized Beam Theory for the analysis of thin-walled circular pipes'. *Thin-Walled Structures*, 173, 109029.
Jin, S., Li, Z., Tang, Q., He, Z., and Huang, H. (2021). 'A combined force/displacement-based constrained finite strip method for modal stability analysis of thin-walled members.' *Thin-Walled Structures*, 159, 107322.
Khezri, M., Abbasi, M., and Rasmussen, K. J. R. (2017). 'Application of the compound strip method in buckling analysis of cold-formed steel built-up sections.' *ce/papers*, 1(2-3), 1667-1676.
Khezri, M., and Rasmussen, K. J. R. (2023). 'Buckling Mode Decomposition of Built-up Members by the Modal Finite Strip Method (mFSM).' *Proceedings of the Annual Stability Conference Structural Stability Research Council*, Charlotte, NC, USA
Khezri, M., and Rasmussen, K. J. R. (2018). 'A generalized strain–energy based approach to buckling mode decomposition of thin-walled members.' *Proceedings of the Eighth International Conference on Thin-Walled Structures*
Khezri, M., and Rasmussen, K. J. R. (2019a). 'An energy-based approach to buckling modal decomposition of thin-walled members with arbitrary cross-sections, Part 2: Modified global torsion modes, examples.' *Thin-Walled Structures*, 138, 518-531.
Khezri, M., and Rasmussen, K. J. R. (2019b). 'An energy-based approach to buckling modal decomposition of thin-walled members with arbitrary cross sections, Part 1: Derivation.' *Thin-Walled Structures*, 138, 496-517.
Plank, R. J., and Wittrick, W. H. (1974). 'Buckling under combined loading of thin, flat-walled structures by a complex finite strip method.' *International Journal for Numerical Methods in Engineering*, 8(2), 323-339.
Rendall, M. A., Hancock, G. J., and Rasmussen, K. J. R. (2017). 'The generalised constrained finite strip method for thin-walled members in shear.' *Thin-Walled Structures*, 117, 294-302.
Strang, G. (1993). 'The fundamental theorem of linear algebra.' *The American Mathematical Monthly*, 100(9), 848-855.
Trahair, N. S. (2017). 'Flexural-torsional buckling of structures'. *CRC press*.
Wiseman, D. L., and Puckett, J. A. (1991). 'Applications of compound strip method for folded plates with connecting elements.' *Journal of Structural Engineering*, 117(1), 268-285.